Molecular and Cellular Pathobiology

Cancer Research

Dual Roles for CXCL4 Chemokines and CXCR3 in Angiogenesis and Invasion of Pancreatic Cancer

Cathy Quemener[1,2], Jessica Baud[1,2], Kevin Boyé[1,2], Alexandre Dubrac[1,2,3], Clotilde Billottet[1,2], Fabienne Soulet[1,2], Florence Darlot[1,2], Laurent Dumartin[1,2], Marie Sire[1,2], Renaud Grepin[1,2], Thomas Daubon[1,2], Fabienne Rayne[2,4], Harald Wodrich[2,4], Anne Couvelard[5], Raphael Pineau[1,2], Martin Schilling[6], Vincent Castronovo[7], Shih-Che Sue[8], Kim Clarke[9], Abderrahim Lomri[1,2], Abdel-Majid Khatib[1,2], Martin Hagedorn[1,2], Hervé Prats[3], and Andreas Bikfalvi[1,2]

Abstract

The CXCL4 paralog CXCL4L1 is a less studied chemokine that has been suggested to exert an antiangiogenic function. However, CXCL4L1 is also expressed in patient tumors, tumor cell lines, and murine xenografts, prompting a more detailed analysis of its role in cancer pathogenesis. We used genetic and antibody-based approaches to attenuate CXCL4L1 in models of pancreatic ductal adenocarcinoma (PDAC). Mechanisms of expression were assessed in cell coculture experiments, murine, and avian xenotransplants, including through an evaluation of CpG methylation and mutation of critical CpG residues. *CXCL4L1* gene expression was increased greatly in primary and metastatic PDAC. We found that myofibroblasts triggered cues in the tumor microenvironment, which led to induction of CXCL4L1 in tumor cells. CXCL4L1 expression was also controlled by epigenetic modifications at critical CpG islands, which were mapped. CXCL4L1 inhibited angiogenesis but also affected tumor development more directly, depending on the tumor cell type. *In vivo* administration of an mAb against CXCL4L1 demonstrated a blockade in the growth of tumors positive for CXCR3, a critical receptor for CXCL4 ligands. Our findings define a protumorigenic role in PDAC development for endogenous CXCL4L1, which is independent of its antiangiogenic function. *Cancer Res; 76(22); 6507–19. ©2016 AACR.*

Introduction

A paralog of CXCL4, named platelet factor variant-1 (PF4v1) or CXCL4L1, was identified in 1989, but its role in cancer progression has not yet been investigated (1, 2). CXCL4L1 and CXCL4 exhibit only 34% differences in the amino terminus encoding the signal sequence and 4.3% difference in the mature protein. CXCL4L1 has been shown to be more potent than CXCL4 at inhibiting cell proliferation and migration (2, 3). Furthermore, inhibition of tumor development was observed in tumors derived from implantation of A549, LLC, and B16 cells in mice, treated with recombinant CXCL4L1 (1). In addition, the secretion and processing mechanisms of CXCL4L1 and CXCL4 are different (4). However, both chemokines are secreted with similar efficiency (3). CXCL4L1 has much lower glycan-binding affinity and better diffusibility *in vitro* and *in vivo* (3). These differences are caused by single amino acid changes, which confer a unique structure to the molecule (3, 5). CXCL4L1 is not only expressed in the platelet megakaryocytic lineage but also in immune cells and in other cell types as well, such as smooth muscle cells and endothelial cells (4). It has been reported that CXCL4L1 interacts with CXCR3B and that its blockade *in vivo* using specific anti-CXCR3 mAbs abrogates the inhibitory effect of CXCL4L1 on corneal angiogenesis in the mouse (6–8). CXCR3 is also expressed in a variety of cell types, including immune cells, vascular cells, and tumor cells. CXCR3 exists as different isoforms, including CXCR3-A, CXCR-B, and CXCR3-alt (7). CXCR3-A has been implicated in chemotactic activity and is highly expressed in Th1-type $CD4^+$ T cells, effector $CD8^+$ T cells, and natural killer cells and exhibits tumor-promoting abilities (9). CXCR3-B, which differs from CXCR3-A by an amino terminal extension, is believed to mediate angiostatic activities (7). These findings suggest that CXCL4L1 has regulatory functions in tumor angiogenesis.

Although some data have been published on the effect of exogenous full-length CXCL4L1 or of a CXCL4L1 C-terminal fragment in subcutaneous tumor models (1, 6, 10–12), nothing is known about its precise role in controlling tumor growth and invasion. We provide herein the first study, to our knowledge, of the regulation of CXCL4L1 expression and the role of endogenous CXCL4L1 in tumor development using pancreatic ductal adenocarcinoma (PDAC) as a tumor model. Furthermore, the results described in this article are also of clinically relevance.

[1]INSERM U1029, Pessac, France. [2]Université Bordeaux, Pessac, France. [3]INSERM U1037, Toulouse, France. [4]CNRS UMR 5234, Pessac, France. [5]Department of Pathology, Hôpital Bichat, Paris, France. [6]Department of Visceral Surgery, University Homburg/Saar, Homburg, Germany. [7]Department of Pathology, University of Liège, Liège, Belgium. [8]Department of Life Science, National Tsing Hua University, Hsinchu, Taiwan. [9]Department of Integrative Biology, University of Liverpool, Liverpool, United Kingdom.

Note: Supplementary data for this article are available at Cancer Research Online (http://cancerres.aacrjournals.org/).

Corresponding Author: Andreas Bikfalvi, INSERM U1029 and University Bordeaux, Allée Geoffroy St Hilaire, Pessac 33615, France. Phone: 335-4000-8703; Fax: 335-4000-8705; E-mail: andreas.bikfalvi@u-bordeaux.fr

doi: 10.1158/0008-5472.CAN-15-2864

Materials and Methods

Cells

Pancreatic tumor cell lines (BxPC3 ATCC CRL-1687), Panc-1 ATCC CRL-1469, MIA PaCa-2 ATCC CRL-1420), human osteosarcoma MG63 cells (ATCC CRL-1427), U87 cell line (ATCC-HTB-14), human umbilical vein endothelial cells (HUVEC, Lonza), human coronary artery smooth muscle cells (SMC, PromoCell), NIH3T3 cells (ATCC CRL-1658), Hek cells (ATCC CRL-1573), human hepatic myofibroblasts (kindly donated by J. Rosenbaum, INSERM U 1034, University Bordeaux, Pessac, France) were grown as described in Supplementary Materials and Methods. The last cell authentication was carried out by PCR single-locus technology (Eurofins, GE, date of report: October 14, 2015).

BxPC3 Panc-1 and MIA PaCa-2 tumor cells were transduced with recombinant lentiviral vectors expressing firefly luciferase. Tumor cell implantation in fertilized chicken eggs (*Gallus gallus*) was handled as described previously (13, 14). Tumor nodule isolation, processing for microarrays, and subsequent analysis are described in ref. 14 and in Supplementary Materials and Methods.

Coculture experiments

BxPC3 cells or PANC-1 cells were cocultured with human liver myofibroblast, HUVEC, or SMC. BxPC3 cells were cocultured for 24 to 96 hours with myofibroblasts on PEN membrane. Laser capture microdissection analyses were performed by using a PALM MicroBeam microdissection system version 4.0–1206 equipped with a P.A.L.M. RoboSoftware (P.A.L.M. Microlaser Technologies, Zeiss). Furthermore, coculture experiments using transwell system (Greiner Bio-One <0.45 μm) with BxPC3 cells and myofibroblasts were used. These experiments were conducted in two ways. Tumor cells (2×10^5) were placed in the upper side of the membrane and myofibroblasts at the lower side in DMEM containing 20% FBS. Alternatively, myofibroblasts were removed after 24 hours and RNA extracted after additional 24 hours and CXCL4L1 expression measured. For details, see Supplementary Materials and Methods.

Isolation of microparticles

Microparticles were isolated from supernatants of myofibroblasts grown to confluency (T75 at confluency). Centrifugation was done at 2,500 rpm for the elimination of cellular fragments (10 minutes). The supernatant was centrifuged at 100,000 × *g* for 1 hour, and the pellet was collected and resuspended in medium before use.

In vivo mouse models

To evidence tumor targeting of MabL1, the antibody was labeled with IRDye and 25 μg of labeled antibodies was injected into the tail vein of mice with subcutaneous BxPC3 tumors or with metastasis after spreading of BxPC3 cells through the portal vein following intrasplenic injection according to standard procedures (15). At different times post-injection, animals were imaged with the Odyssey Imaging System (LI-COR).

For xenograft models, 8-week-old mice were anaesthetized with intraperitoneal injection of ketamine (150 mg/kg) and xylazine (15 mg/kg) and xenografted with 3×10^6, 1×10^6, and 3.75×10^5 BxPC3, Panc-1, or MIA PaCa-2 cells stably transfected with a luciferase reporter gene in 100 μL serum-free medium by subcutaneous, intrapancreatic, and intrasplenic injection, respectively. Treatment with MabL1 antibody was carried according to standard procedures (15). Tumor volumes were measured by caliper or bioluminescence (Photon Imager, Biospace Lab). For more details, see Supplementary Materials and Methods.

All other methods were carried out according to standard procedures (references below) and are detailed in the Supplementary Materials and Methods. These include reagents; siRNA transfection with Lipofectamine (Invitrogen, according to the manufacturer's instructions); cell proliferation and invasion assay (16); Western blotting and immunoprecipitation (17, 18); RNA extraction and semiquantitative and quantitative RT-PCR (18); histology, IHC, and tissue microarray (TMA; refs. 18); *in situ* hybridization (Roche RNA Labeling Kit SP6/T7, according to the manufacturer's instructions), labeling of MabL1 (IRDye 800CW, Protein Labeling Kit-HighMW#928-38040, LI-COR); construction of luciferase reporter vectors luciferase reporter assay (Promega, according to the manufacturer's instructions); *in vitro* methylation of plasmid DNA and bisulfite sequencing (New England Biolabs, according to the manufacturer's instructions); and clearance kinetic of MabL1 conjugated to IRDye or biotin.

In silico and statistical analysis

In silico online research was done on Oncomine (https://www.oncomine.org) and The Cancer Genome Atlas (TCGA; cancergenome.nih.gov) datasets.

Experimental data. Results are presented as mean ± SEM. Statistical significance was determined by a one-tailed, unpaired Student *t* test using Prism 5.03 GraphPad Software. For the TMAs, the statistical analysis was performed by using a Kruskal–Wallis test, followed by Dunn multiple comparison procedure. $P < 0.05$ was considered significant (***, <0.001; **, <0.01; *, <0.05).

Ethical issues

Male RAG-γ/c mice were housed and treated in the animal facility of Bordeaux University (Animalerie Mutualisée Bordeaux). All animal procedures have been done according to the institutional guidelines and approved by the local ethics committee.

Fresh human adenocarcinoma samples were provided by Prof. Martin Schilling (Klinik für Allgemeine Chirurgie, Viszeral-, Gefäß- und Kinderchirurgie, Homburg, Germany). Fresh tumor tissues were obtained during surgery and directly snap-frozen in liquid nitrogen. TMAs were provided by Prof. Anne Couvelard (Hôpital Bichat, Paris, France). Patients gave their consent prior tissue analysis according to the clinical guidelines.

Results

Expression of CXCL4L1 or CXCL4 in pancreatic adenocarcinoma

Transcriptomic profiling identifies CXCL4L1 but not CXCL4 in the PDAC-CAM model. Dual transcriptomic analysis using human Affymetrix or chicken Affymetrix microarrays was performed between tumor day 1 (T1) and tumor day 6 (T6) of BxPC3 cells implanted onto the chick chorioallantoic membrane (CAM; E11 and E16 of embryonic development; ref. 14). CXCL4L1 was

upregulated at T6 compared with T1 (a 14-fold increase) in human Affymetrix arrays.

Real-time PCR (SYBR Green) revealed significant CXCL4L1 expression in T6 tumors when compared with T1 CAM tumors (9.7-fold). No expression was seen in BxPC3 cells *in vitro* (Fig. 1A). When TaqMan for RT-PCR was used, a very small amount of CXCL4 was detected in BxPC3 cells but only at 37 cycles (CT). CXCL4L1 was never detected in BxPC3 cells cultured under these conditions.

An mAb (MabL1) specific for CXCL4L1 revealed immunoreactivity in T6 CAM tumors (Fig. 1B), and CXCL4L1 protein was also detected by Western blotting (Fig. 1C). *In situ* hybridization demonstrated CXCL4L1 but not CXCL4 expression in T6 CAM tumors (Fig. 1D).

Expression analysis in mouse models of pancreatic carcinoma. CXCL4L1 is expressed in BxPC3 tumors grown in mice (Fig. 1E, left) in the primary tumor and lung metastasis (Fig. 1F, top). In contrast to BxPC3, some CXCL4L1 expression was already detected in Panc-1 cells in culture. However, similar to BxPC3, expression was further increased (4.49-fold) when cells were implanted into mice (Fig. 1E, middle and F, lower middle). The effect of the microenvironment is specific to CXCL4L1 and does not occur for CXCL4. Furthermore, BxPC3 grafts form lung micrometastases (average size: 0.024 mm^2, $n = 10$), whereas Panc-1 grafts form larger metastases (average size: 0.15 mm^2, $n = 8$).

The situation was different for MIA PaCa-2, another PDAC cell line (Fig. 1E and F, right). In this case, cells merely express CXCL4, but not CXCL4L1, at significant levels *in vitro*. In xenograft tumors, CXCL4 was further increased and CXCL4L1 became detectable.

Thus, the expression profile *in vitro* and *in vivo* is heterogeneous in these three PDAC cell line.

Expression analysis of CXCL4L1/CXCL4 in human tumor samples. CXCL4L1 is merely expressed in fetal liver, colon, and to some extent in spleen; CXCL4 is highly expressed in spleen (Supplementary Fig. S1A). Normal human pancreas comparatively does not express elevated levels of CXCL4L1 or CXCL4 mRNA.

CXCL4L1 mRNA was overexpressed in 33 of 33 samples from human PDAC patients (median $\log_2$ of 2.55 corresponding to a median of 5.85; Supplementary Fig. S1B). CXCL4L1 protein was detected in primary pancreatic tumors and metastasis (Supplementary Fig. S1C–S1E). CXCL4 was expressed in patient samples, but at lower expression levels than CXCL4L1 (Supplementary Fig. S1B right, and S1F).

In the TMA, increased CXCL4L1 immunoreactivity was significantly associated with pancreatic adenocarcinoma ($P < 0.001$; Supplementary Fig. S1G–S1O). A statistically significant increase was also observed in adenosquamous tumors and chronic pancreatitis ($P < 0.05$).

CXCL4L1 expression is significantly higher in PDAC in comparison with control in the Segara Pancreatic statistics (19). In the Stratford and Yeh dataset (GSE21501), survival was significantly linked to CXCL4L1 expression ($P = 0.023$). In the TCGA dataset (cancergenome.nih.gov), statistical significance was >0.05, probably due to the insufficient amount of patients included in the analysis (Supplementary Fig. S2).

The Ishikawa Pancreas statistics (20; left panel) was used to compare *CXCL4* gene expression in pancreas or in pancreatic ductal adenocarcinoma. Survival analysis (right panel) did not show a significant link to survival in the TCGA pancreatic cancer cohort ($P = 0.096$; Supplementary Fig. S2).

Thus, these data suggest that tumor-derived CXCL4L1, but not CXCL4, is a possible marker for the clinical evolution of PDAC.

Cellular and molecular analysis of CXCL4L1 expression

We focused all of our subsequent analyses on CXCL4L1.

We reasoned that some microenvironmental cues could induce CXCL4L1 expression. We therefore cocultured BxPC3 cells with endothelial cells (HUVECs, HUACs), human SMCs, NIH 3T3 cells, or myofibroblasts. None of the cell types was able to induce CXCL4L1 expression in BxPC3 cells except myofibroblasts (Fig. 2A and B). For VAMP2, colocalization was observed but to a lesser extent (Pearson coefficient, 0.67; Fig. 2C).

Coculturing BxPC3 cells with myofibroblasts in the transwell system revealed significant induction of CXCL4L1 in tumor cells. Microparticles from the myofibroblast-conditioned medium (CM) were able to increase CXCL4L1 expression to some extent, albeit much lower than the complete CM (Fig. 2D).

These results indicate that a paracrine factor derived from myofibroblasts is able to increase CXCL4L1 expression in tumor cells. The majority of this factor is soluble and a fraction is also contained in microparticles.

We also demonstrated that expression of CXCL4L1 is reversible in BxPC3 cells after removal of myofibroblasts from the transwell chamber (Fig. 2E). However, coculturing myofibroblasts with PANC-1 in the transwell system could not further increase CXCL4L1 expression (Supplementary Fig. S3A). Thus, myofibroblasts may provide the initial trigger for CXCL4L1 expression, but additional factors may be required for full stimulation.

Myofibroblasts express, by their own, high levels of vimentin and FAP and low levels of FSP1 and both chemokines (Supplementary Fig. S3B).

We next focused on epigenetic modifications that might be involved in CXCL4L1 expression. The *CXCL4L1* gene is located within a cluster of chemokines-encoded genes (Fig. 3A). To determine the expression of these genes and to examine the putative influence of CpG islands methylation, BxPC3 cells were stimulated with 5′-Aza, a potent DNA methyltransferase inhibitor, and with or without the histone deacetylase inhibitor, trichostatin A (TSA; Fig. 3B). Treatment with 5′Aza or TSA increased the level of CXCL4L1 mRNA in BxPC3 cells (Fig. 3B, left). In contrast, no changes were observed in CXCL1 and CXCL6 expression with this treatment. This indicates that DNA methylation is involved in the silencing of the *CXCL4L1* gene in BxPC3 cells.

Using the MethPrimer website, one CpG island was found to be located within the first intron (Fig. 3C). Bisulfite sequencing indicated that two of eight sites (+150, +193, +210, +212, + 214, +227, +250, and +259) were demethylated in the presence of 5′Aza [CpG 6 (+227) and CpG 7 (+250)], the CpG site number referring to the transcription start site (Fig. 3D). All 7 sequences from the most hypomethylated lung metastasis showed hypomethylation of the two CpG sites. Globally, hypomethylation at CpG 6 and 7 was of 58.75% ± 13.38 SD ($n = 5$ metastases). In the most hypomethylated subcutaneous primary tumors, the majority of sequences (4/7) showed

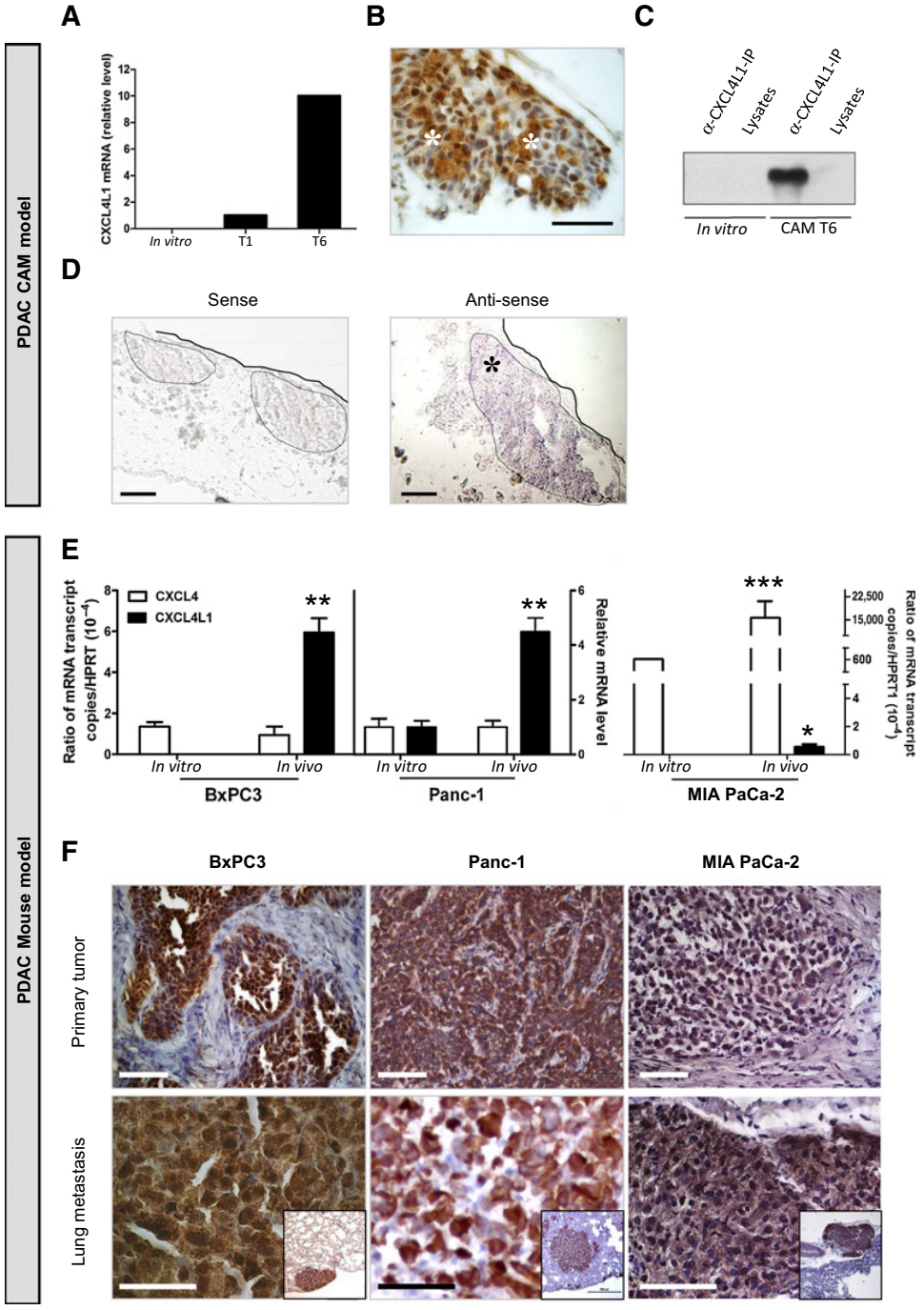

Figure 1.

CXCL4L1 expression in the PDAC-CAM and mouse xenograft model. **A,** *CXCL4L1* expression in BxPC3 cells *in vitro* and in the PDAC-CAM model at day 1 (T1) and day 6 (T6), normalized to S16 expression. *CXCL4L1* mRNA at T1 with arbitrary value 1. **B,** immunolabeling on T6 CAM with MabL1. **C,** Western blotting for CXCL4L1 from pooled T6 CAM lysates ($n = 3$) or BxPC3 cells lysates with MabL1. The gel is representative of two independent experiments. **D,** *in situ* hybridization of T6 PDAC-CAM samples with *CXCL4L1* riboprobes. Dotted lines, tumor nodes; full lines, CAM surface. **E,** qRT-PCR from mRNA of BXPC3, Panc-1, and MIA PaCa-2 cells in culture ($n = 4$) or of tumors derived from subcutaneously injected cells ($n = 8$ tumors; **, $P < 0.01$; ***, $P < 0.001$). **F,** CXCL4L1 immunolabeling of BxPC3 (subcutaneous), Panc-1, and MIA PaCa-2 tumors (orthotopic) and lung metastasis. Global view (inset). Scale bars, 50 μm (primary tumors) and 100 μm (lung metastasis). Error bars, SEM. *, positive node.

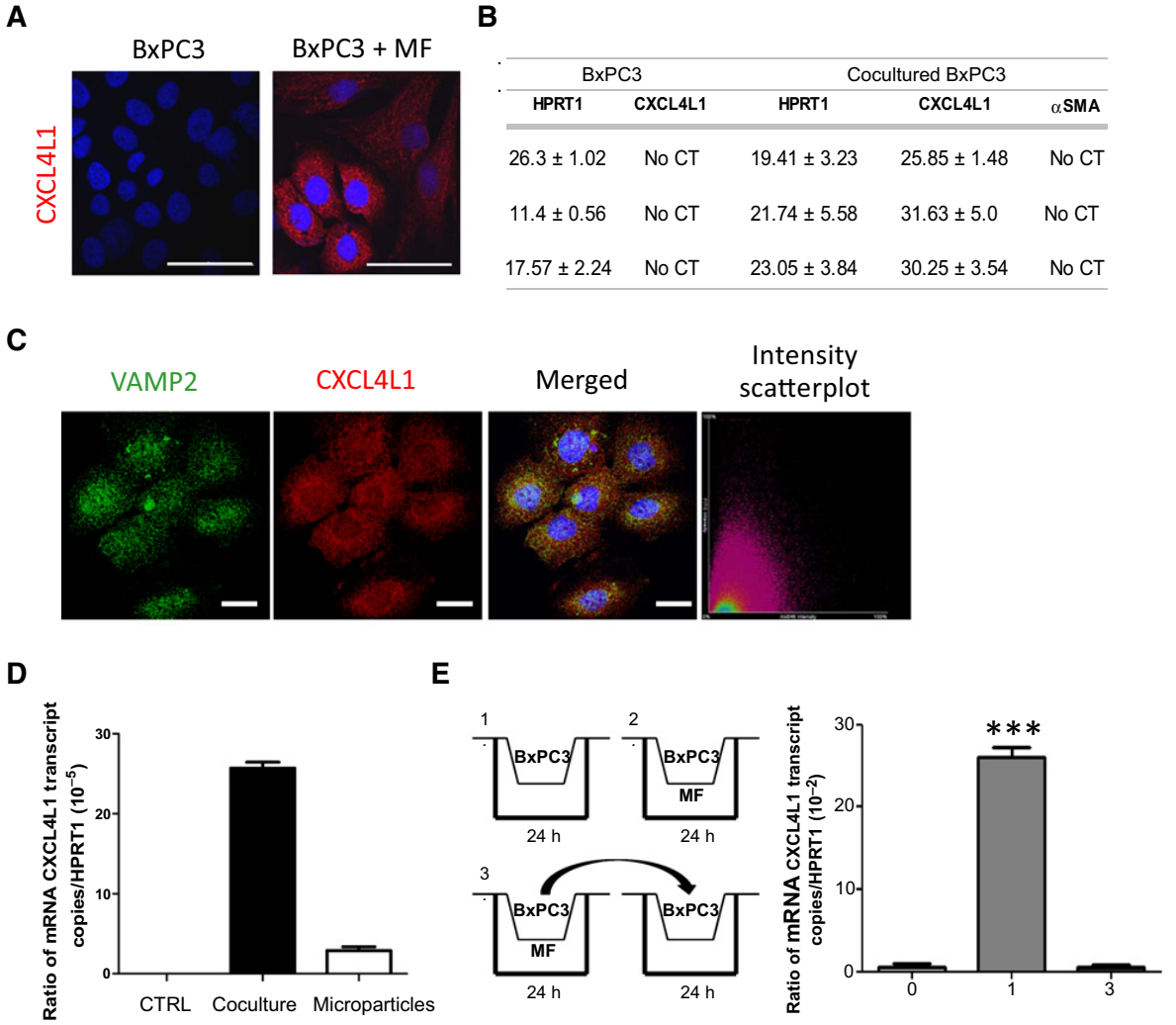

Figure 2.

Coculture of tumor cells with myofibroblasts. **A,** immunofluorescence staining for CXCL4L1 on BxPC3 cells alone (left) or cocultured for 4 days with myofibroblasts (MF; right). Blue, DAPI-labeled nuclei. **B,** qRT-PCR from laser microdissected BxPC3 cell mRNA. Data as CT value as means ± SD of five microdissected samples. *HPRT1* as a housekeeping gene and α-*SMA* as a control for contamination by myofibroblasts. **C,** immunofluorescence staining on cocultured BxPC3 for CXCL4L1 and VAMP-2. Blue, DAPI-labeled nuclei. Merged staining (yellow) revealed areas of colocalization and scatter 2D plots of intensities in red and green immunofluorescence channels (NIS software). **D,** BxPC3 cells (2×10^5) were cocultured using transwell system with myofibroblasts (2×10^5) for 24 hours or with microparticles. mRNA was extracted and analyzed by qPCR for CXCL4L1 expression. Data as copy number/HPRT. Scale bar, 50 μm (**A**) and 10 μm (**C**). **E,** BxPC3 cells (2×10^5) were cocultured using a transwell system with myofibroblasts (2×10^5) for 24 hours. Myofibroblasts were then removed from the transwell chamber for 24 hours. mRNA was then extracted and analyzed by qPCR for CXCL4L1 expression. Data as copy number/HPRT. ***, $P < 0.001$.

hypomethylation. However, this was not uniform for all tumors examined and some variability was observed. Globally, hypomethylation was of 25.09% ± 4.45 SD ($n = 8$ subcutaneous tumors). This correlates with the induction of expression of CXCL4L1 (Fig. 3D, right).

In patients ($n = 10$), for all 8 methylation sites, 69.38% ± 4.9 SD hypomethylation was observed (Fig. 3D). For CpG 6 (+227) and CpG 7 (+250), this percentage was of 74.60% ± 7.3 SD. Thus, the majority of sequences demonstrate hypomethylation at site CpG 6 (+227) and CpG 7 (+250), which is in agreement with results observed with the cell line. It is to emphasize that DNA from the entire tumor tissue was analyzed, which also includes tumor stroma and some normal pancreatic tissue.

To determine whether CpG 6 (+227) and CpG 7 (+250) are involved in the induction of CXCL4L1, CpG 6 (+227) and CpG 7 (+250) were mutated (C→T). After *in vitro* methylation followed by transfection, a Luc reporter assay was performed. The ratio of LucF/LucR was highly increased when CpG 6 (+227) and CpG 7 (+250) were mutated when compared with the nonmutated wild type (Fig. 3E).

Short-term stimulation with IL1β was unable to induce CXCL4L1 expression in BxPC3 cells, in contrast to what was

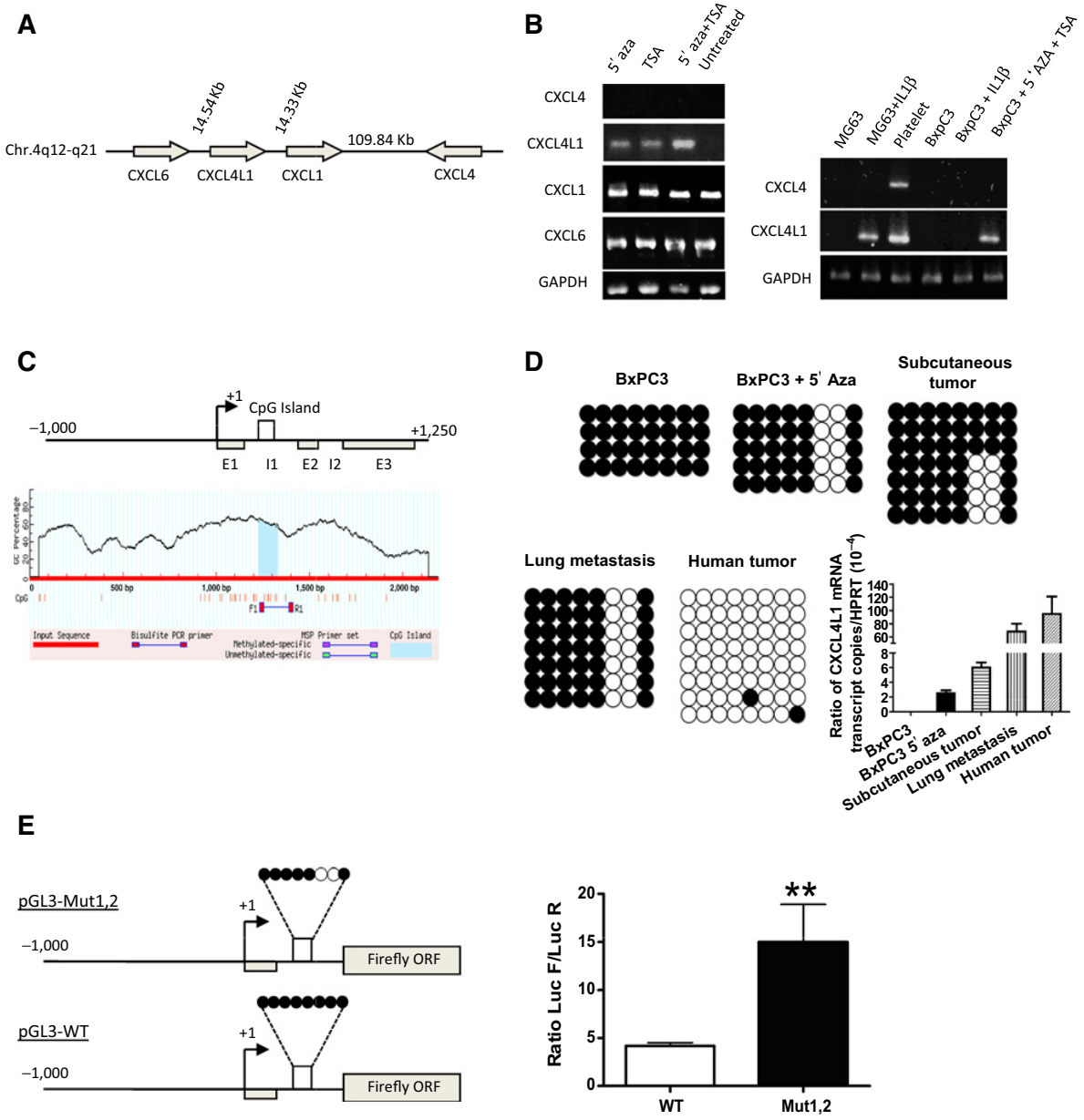

Figure 3.

Modulation of *CXCL4L1* expression by DNA methylation. **A,** *CXCL4L1* and *CXCL4* genomic organization. **B,** RT-PCR analyses of *CXCL4, CXCL4L1, CXCL1*, and *CXCL5* mRNA from BxPC3 cells treated with 5′-Aza and/or TSA (left). RT-PCR analyses of *CXCL4* and *CXCL4L1* mRNA from platelets, BxPC3, and MG63 cells treated with IL1β and 5′-Aza/TSA (right). *GAPDH* as an internal control. **C,** location of CpG sites (vertical bars); bisulfite sequencing primers in the first intron with the MethPrimer website. **D,** methylation of *CXCL4L1* in BxPC3 cells treated or untreated with 5′-Aza in BxPC3 subcutaneous primary tumors and in lung metastases from mice injected with BxPC3 into the spleen (one representative tumor and metastasis, $n = 10$ tumors/group; left). Filled and open circles, methylated and unmethylated CpG sites, respectively. qRT-PCR of C*XCL4L11* mRNA from 5′-Aza–treated or untreated BxPC3 cells and from subcutaneous tumor and lung metastasis (right). *HPRT1,* internal control. ($n = 6$ samples/group). **E,** characterization of *CXCL4L1* expression. The 1-kb upstream promoter, exon 1, and intron 1 regions of human *CXCL4L1* cloned in front of the *luciferase* firefly gene. Wild-type sequence (WT) or mutated sequence in the two CpG sites regulated by the 5′Aza treatment. After *in vitro* methylation and transfection, the ratio of LucFirefly/Luc*Renilla* was determined ($n = 3$; **, $P < 0.01$). Error bars, SEM.

observed in MG63 osteosarcoma cells (see Fig. 3B, right; ref. 10). Long-term stimulation with IL1β was reported to trigger demethylation (21) but was unable to increase CXCL4L1 in PDAC.

Expression of CXCR3 in pancreatic adenocarcinoma

High expression of CXCR3-A mRNA was seen in Panc-1 cells (Fig. 4A) but no expression in BXPC3 or MIA PaCa-2 cells. Some CXCR3-B mRNA was detected in Panc-1 cells, and low

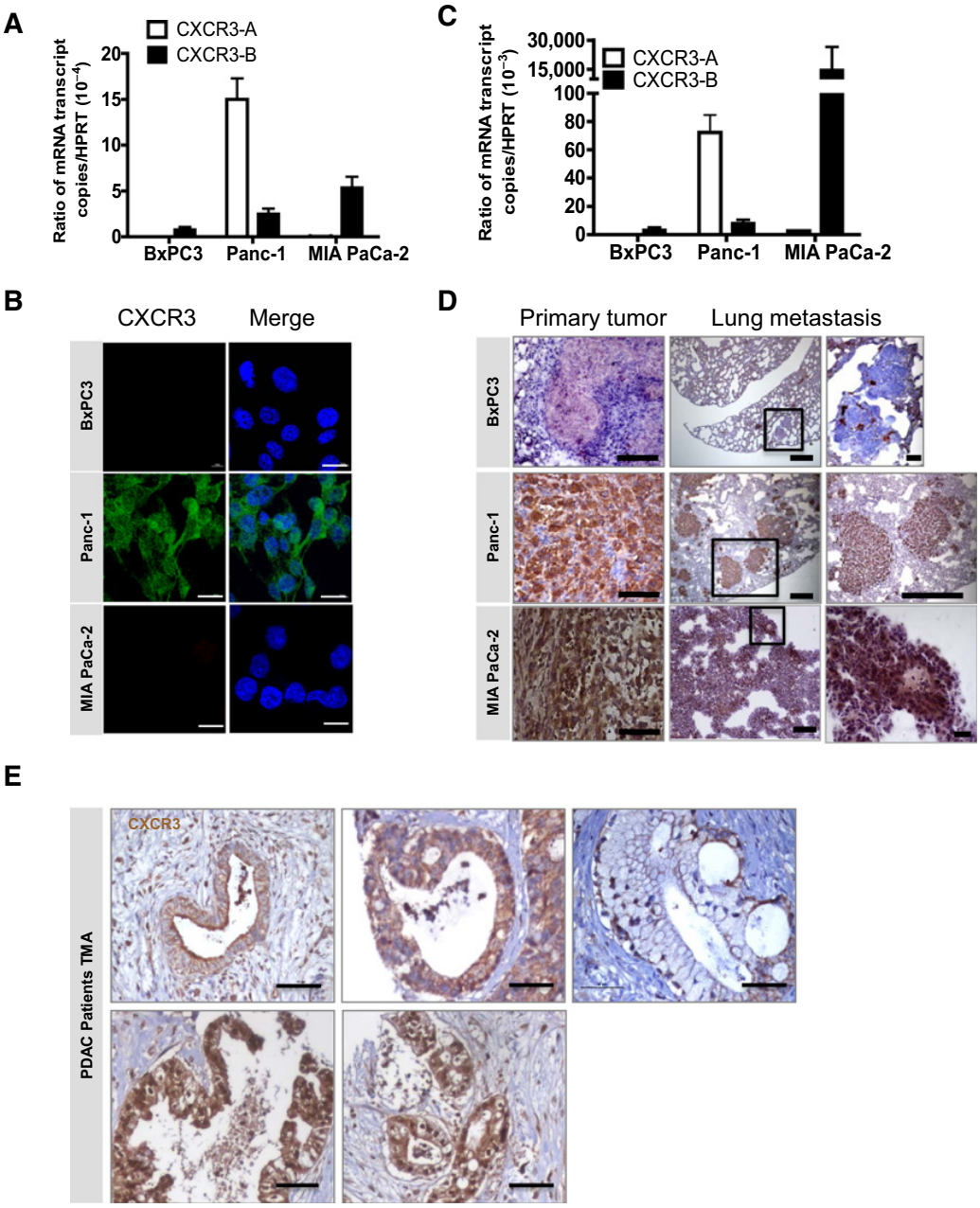

Figure 4.

Expression of CXCR3 in pancreatic adenocarcinoma. **A,** qRT-PCR for CXCR3-A and CXCR3-B. **B,** immunofluorescence staining *in vitro*. **C,** qRT-PCR for *CXCR3-A* and *-B* in primary tumors from BxPC3, PANC-1, and MIA PaCa-2 cells implanted mice ($n = 12$ and 10 tumors/group). **D,** immunostaining for human CXCR3 of subcutaneous BxPC3 and orthotopic PANC-1 and MIA PaCa-2 tumors (left) and lung metastasis (middle and right). **E,** IHC for CXCR3 (brown) and hematoxylin counterstaining (blue) of PDAC patients' TMA showing apical (top left), cytoplasmic (top middle), membrane (top right), and nuclear staining (bottom). Scale bars, 20 μm (**B**), 100 μm (**D**, left and bottom right), 500 μm (**D**, middle), and 50 μm (**D**, top right; **E**). Error bars, SEM.

mRNA expression was also seen in BxPC3 and MIA PaCa-2 cells. However, no CXCR3 protein expression was seen in BxPC3 and MIA PaCa-2 cells *in vitro* in contrast to Panc-1 (Fig. 4B).

When Panc-1 cells were implanted subcutaneously or orthotopically into mice, a strong increase of mRNA expression was observed for CXCR3-A and CXCR-B (50-fold and 35-fold increase respectively, Fig. 4C). Positive immunoreactivity for CXCR3 was also evidenced in these tumors (Fig. 4D). For MIA PaCa-2 cells, after *in vivo* implantation, CXCR3-B was highly expressed (Fig. 4C and D) and much higher than *in vitro* (copy number ratio CXCR3/HPRT *in vivo*: $14,687 \pm 0.011$ versus $5.39 \times 10^{-4} \pm 1.1 \times 10^{-4}$ *in vitro*). Metastatic foci were also positive for CXCR3. On the contrary, BxPC3 cells do not significantly express CXCR3-A and -B *in vivo*.

Seventy PDAC samples included in TMAs were then analyzed. The cytoplasmic and nuclear scores ranged from 20 to 300 (median: 175) and from 0 to 300 (median: 175), respectively (Fig. 4E). Twenty-two (31%) of the tumors presented a membranous staining pattern, some of which had cytoplasmic staining (Fig. 4E). CXCR3 nuclear and membranous expression correlated positively with tumor size ($P = 0.02$ and $P = 0.06$, respectively). CXCR3 membranous expression correlated with the presence of perineural invasion ($P = 0.04$).

We furthermore performed an *in silico* analysis of CXCR3 expression using the Ramaswamy multicancer set (22) and the Bucholz pancreas dataset (Supplementary Fig. S4; ref. 23). In the Ramaswamy dataset, high expression of CXCR3 could be evidenced in PDAC, a finding that is further confirmed in the Bucholz dataset where expression is also significantly increased in PDAC compared with normal pancreas.

In vitro and *in vivo* functional studies

In vitro effects of CXCL4L1. CXCL4L1 inhibited endothelial cell but not BXPC3 cell proliferation (Fig. 5A and B, left; ref. 3). Invasion of endothelial cells, but not that of BxPC3 cells, was significantly inhibited by CXCL4L1 (Fig. 5A, middle, and B, right). No effect on apoptosis on either tumor or endothelial cells was seen (Supplementary Fig. S5).

We verified, in addition, CXCR3 expression in HUVECs, which is indeed significantly expressed (Fig. 5A, right).

We next compared the role of CXCL4L1 in another pancreatic cancer cell line, Panc-1 cells, which, in contrast to BxPC3 cells, do express CXCR3 protein (Fig. 4C and D). This cell line already expresses CXCL4L1 in cell culture (Fig. 1E). Blocking by either CXCL4L1 mAb or siRNA against CXCL4L1 as well as CXCR3 led to the inhibition of cell proliferation (Fig. 5C). Combining blockade by MabL1 and CXCR3 siRNA further decreased cell proliferation. This indicates that CXCL4L1 is a positive regulator of Panc-1 growth and that CXCR3 is also involved in the growth-promoting activity.

As Panc-1 cells express CXCR3, we wanted to investigate whether signaling induced by CXCL4L1 is modulated (Fig. 5D). Indeed, ERK phosphorylation was increased after CXCL4L1 treatment. This increase could be blocked by U1026, a specific inhibitor of MAP kinases.

Effect of endogenous CXCL4L1 on tumor development. RAG-γ/c mice were inoculated subcutaneously with BxPC3 or Panc-1 cells and then treated with MabL1 antibody. Prior to the tumor experiments, we characterize the half-life, clearance, and tumor targeting of this antibody in mice (Supplementary Fig. S6A–S6E; Supplementary Materials and Methods).

We next investigated whether MabL1 was able to target tumor lesions in mice (Fig. 6A–F). BxPC3 cells were injected in the spleen (1×10^6 cells) in mice. Tumors usually occurred at 2 months postinjection. Infrared dye–labeled MabL1 antibody was administered by intravenous injection. Imaging of organs revealed targeting of the antibody to metastatic lesions in the lung and kidney.

In BxPC3 tumor xenografts, injection of MabL1 in mice yielded an increase in tumor growth (Fig. 7A). MabL1 (25 μg) was injected twice a week, and tumor growth was monitored during a 2-month period. Forty-eight days after implantation, tumor size increased by 2-fold in MabL1-treated animals when compared with nontreated controls (2,612 mm^3 in MabL1-treated mice vs. 1,184 mm^3 in control mice). Tumor weight was also increased after antibody treatment (Fig. 7B). The kinetics of tumor growth in MabL1-treated mice was 81.5 mm^3 per day in comparison with 34.9 mm^3 per day in untreated controls. An increase in the density of small vessels was observed in treated tumors compatible with an angiogenesis-related effect (Fig. 7C and D). The vessel increase in MabL1-treated tumor was not accompanied by variation in $NG2^+$ cell coverage (Fig. 7E).

In Panc-1 tumor xenografts, the administration of CXCL4L1 antibody had an opposite effect (Fig. 7F and G). Using the same treatment protocol as for BxPC3 cells, administration of the MabL1 antibody led to a reduction of tumor size in both subcutaneously and orthotopically implanted tumors (subcutaneous implantation: 1,140 mm^3 in MabL1-treated mice vs. 1,845 mm^3 in control mice; orthotopic implantation: 2.8e+06 cpm in MabL1-treated mice vs. 1.25e+07 cpm in control mice). Tumor weight was reduced in both orthotopic and subcutaneous tumors in the presence of MabL1 (Fig. 7H). Lung metastasis as measured by the presence of hS16 mRNA was significantly reduced in orthotopic tumors (Fig. 7I). Furthermore, proliferation measured by hMIB1 expression and Ki67 staining was decreased in orthotopic tumors after MabL1 injection (Fig. 7J and L). However, no effect on vessel quantity as measured by PCAM1 expression was seen (Fig. 7K and L).

Taken together, these results point to an opposite effect of CXCL4L1 in these two pancreatic tumor cell lines, which correlates with the presence of CXCR3 on tumor cells.

We next performed qPCR analysis for PECAM1 in Panc-1 and MIA PaCa-2 tumor samples (Supplementary Fig. S7A). Panc-1 cells express CXCL4L1 contrary to MIA PaCa-2 cells. Supplementary Figure S7A clearly shows that PECAM1 levels were much reduced in Panc1 in comparison with MIA PaCa-2 cells (6.16-fold), and this was inversely correlated with CXCL4L1 expression. Furthermore, we analyzed mouse CXCR3 expression in both tumor types (Supplementary Fig. S7B). Primers are only detecting stroma-derived CXCR3 but no tumor-derived CXCR3. As seen in the figure, this correlated well with PECAM1 expression and inversely with CXCR3 expression (6.16-fold in both cases). In addition, the figure shows that CXCL4L1 is 11 times more expressed in Panc-1 tumors when compared with healthy control pancreas (Supplementary Fig. S7B).

Modulation of CXCR3 in PDAC cells

To study the impact of CXCR3-A, we focused on MIA PaCa-2 cells, as Panc-1 cell knockdown or overexpression was unsuccessful. CXCR3-A was cloned into pGFPN2 vector and stable clones

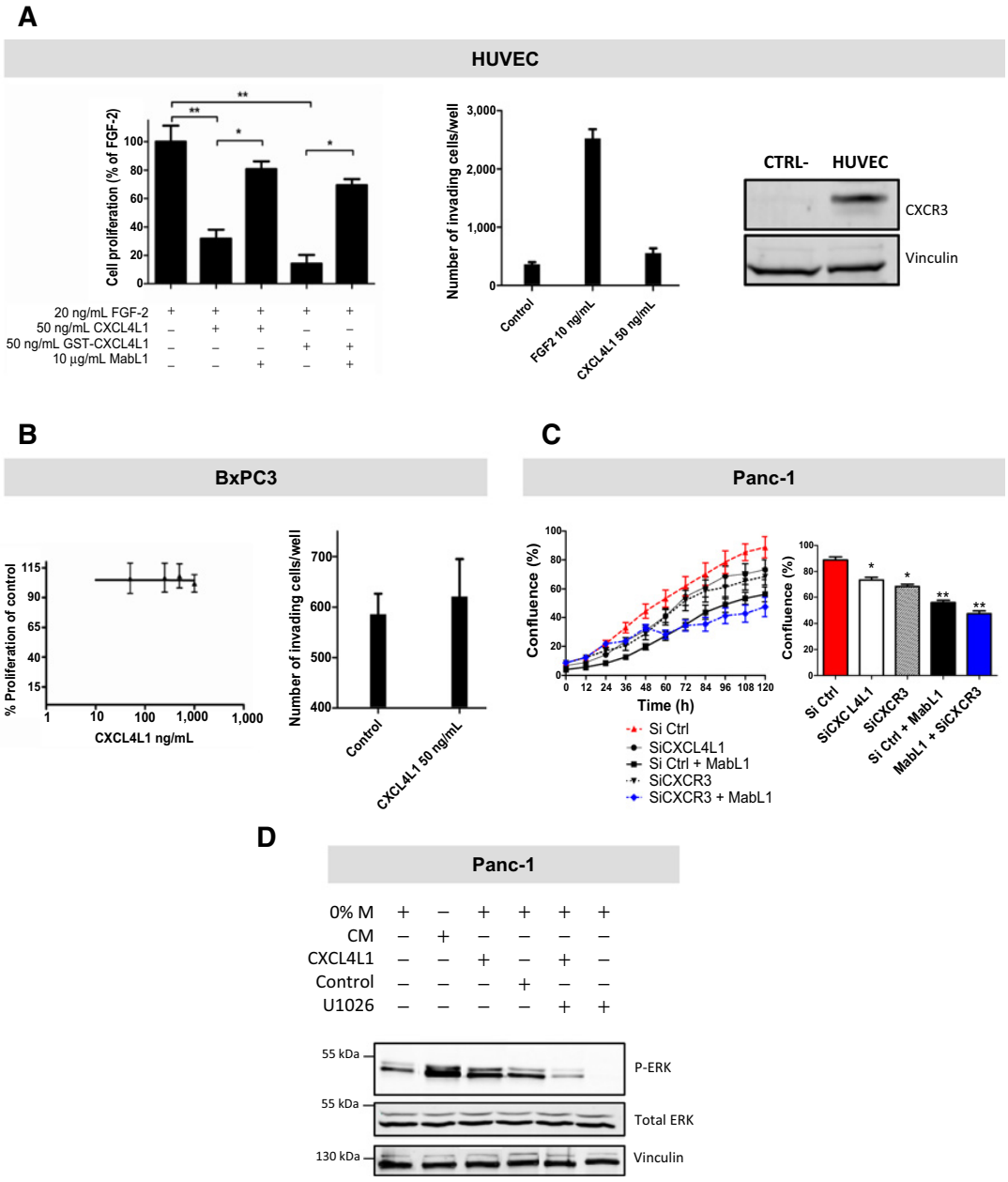

Figure 5.

Functional studies of CXCL4L1 in pancreatic adenocarcinoma and endothelial cells. **A,** activity of recombinant GST-CXCL4L1 and cleaved CXCL4L1 on HUVEC proliferation after 48 hours (left). Endothelial cells cultured with FGF2 (20 ng/mL) and 50 ng/mL of recombinant proteins in the presence of MabL1 (10 µg/mL) or of an IgG control antibody. Effect of recombinant CXCL4L1 (GST-CXCL4L1) on FGF2-stimulated (10 ng/mL) proliferation or invasion of HUVECs (proliferation, left; invasion, middle). CXCR3 protein expression assessed by Western blot analysis in HUVEC cells (right). Vinculin was used as a loading control. **B,** BXPC3 cells (proliferation, left; invasion, right) in the presence of CXCL4L1. **C,** effect of CXCL4L1 and CXCR3 knockdown or antibody treatment on the proliferation of Panc-1 cells. Cells transfected with the specific siRNAs or control siRNAs, grown in complete medium, and treated or untreated with the monoclonal anti-CXCL4L1 antibody over 120 hours. Results as average ± SEM of three independent experiments done in triplicates; ** $P < 0.01$; *, $P < 0.05$. **D,** effect of CXCL4L1 on signaling in Panc-1 cells. Cells stimulated with minimal medium from CXCL4L1-infected cells (MIA PaCa-2) containing >300 ng/mL CXCL4L1 and ERK phosphorylation measured by Western blotting with and without a specific inhibitor of MAP kinases (U1026, 50 µmol/L). 0% M, serum-free medium; CM, complete medium.

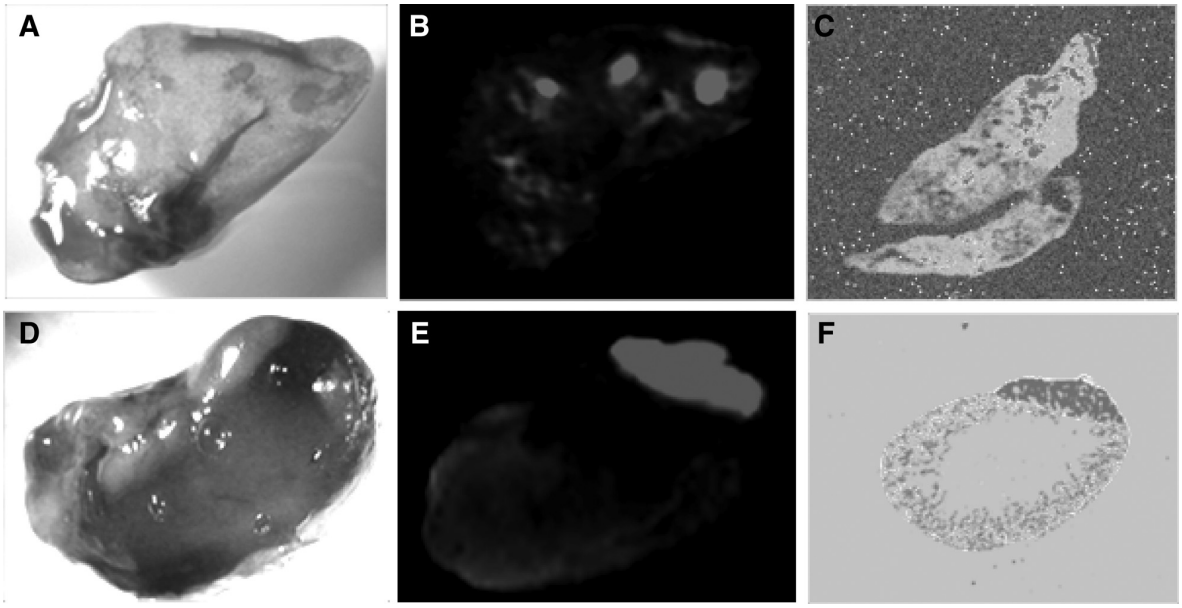

Figure 6.
Targeting of monoclonal MabL1 to tumor lesion in mice. Antibodies labeled with IRDye (MabL1-IRdye) and injected into the tail vein in tumor-bearing mice. Six days after MabI1-IRdye injection, tissues were removed after sacrifice and imaged on the Odyssey Imaging System, frozen, cut into 40-μm sections, and imaged again. Lesions targeted by MabL1 are shown in the lung (**A–C**) and kidney (**D–F**). **C** and **F** depict images of frozen sections.

were isolated. Very high expression levels were observed (copy number 574,943 for CXCR3-A/HPRT; Supplementary Fig. S8A). Cells were also positive by immunodetection (Supplementary Fig. S8B).

We next investigated the functionality of CXCR3 in the condition of chronic stimulation (Supplementary Figs. S8C and S9A–S9C). Only CXCL4L1 produced in Hek cells (Hek-CXCL4L1) stimulated proliferation of MIA PaCa-2-CXCR3 cells. We verified that this effect is dependent on CXCL4L1 and CXCR3 by using MabL1 and SCH546738, a specific high-affinity antagonist of CXCR3, which demonstrated that this is indeed the case (Supplementary Fig. S9B). We also verified the signaling ability and demonstrated that chemokine stimulation induced ERK phosphorylation (Supplementary Fig. S9C).

Orthotopic implantation of MIA PaCa-2-CXCR3 cells did not show a difference in tumor weight when compared with control vector-transfected MIA PaCa-2 cells at sacrifice (day 34 after implantation; Supplementary Fig. S9D). However, the number of lung metastases was increased [human HPRT-1/mouse HPRT-1 by qPCR; 3.5 ± 0.86 (controls) versus 7.3 ± 1.46 (CXCR3-A overexpressors; Supplementary Fig. S9E)]. As MIA PaCa-2 cells did not show significant elevation of CXCL4L1 expression when compared with BxPC3 or Panc-1 cells, we did not perform inhibition studies using the blocking antibody (MabL1). Despite the fact that tumor weight was not modified, changes in hypoxia signature and MMP9 were observed (Supplementary Fig. S9F) in cells that overexpress CXCR3-A. This indicates that CXCR3 has *in vivo* intrinsically, in the absence of CXCL4L1, prometastatic abilities in pancreatic tumor cells.

Discussion

Our data show that tumor cells upregulate CXCL4L1 expression when placed in a suitable microenvironment. Myofibroblasts mimic the *in vivo* microenvironment and were able to induce expression of CXCL4L1. Among potential factors, IL1β was reported to induce promoter demethylation after long-term exposure (21). However, IL1β did not induce CXCL4L1 expression in PDAC cells after short- or long-term exposure. Microparticles from myofibroblast-conditioned medium induced CXCL4L1 expression in tumor cells. However, the effect of the microparticle preparation was much less when compared with chronic exposure in the coculture system. This indicates that a yet nonidentified soluble factor is involved in the induction of CXCL4L1 expression in PDAC cells.

We demonstrated that epigenetic modifications through methylation play a critical role in the induction of CXCL4L1 in tumor cells similar to what has been reported for some other angiogenic factors, receptors, or chemokines, such as maspin (24), intercellular adhesion molecule-1 (ICAM-1) (25), or CXCL12 (SDF1; refs. 26, 27). We found that human PDAC tumors are usually hypomethylated on all eight methylation sites of the CpG island identified, of which two are involved in the induction of CXCL4L1 expression. This is in contrast to many genes where methylation follows tumor progression. However, hypomethylation during tumor progression has also been reported for other genes, including urokinase-type plasminogen activator (28), maspin (29), or matrix metalloproteinases (30), which is in line with our findings.

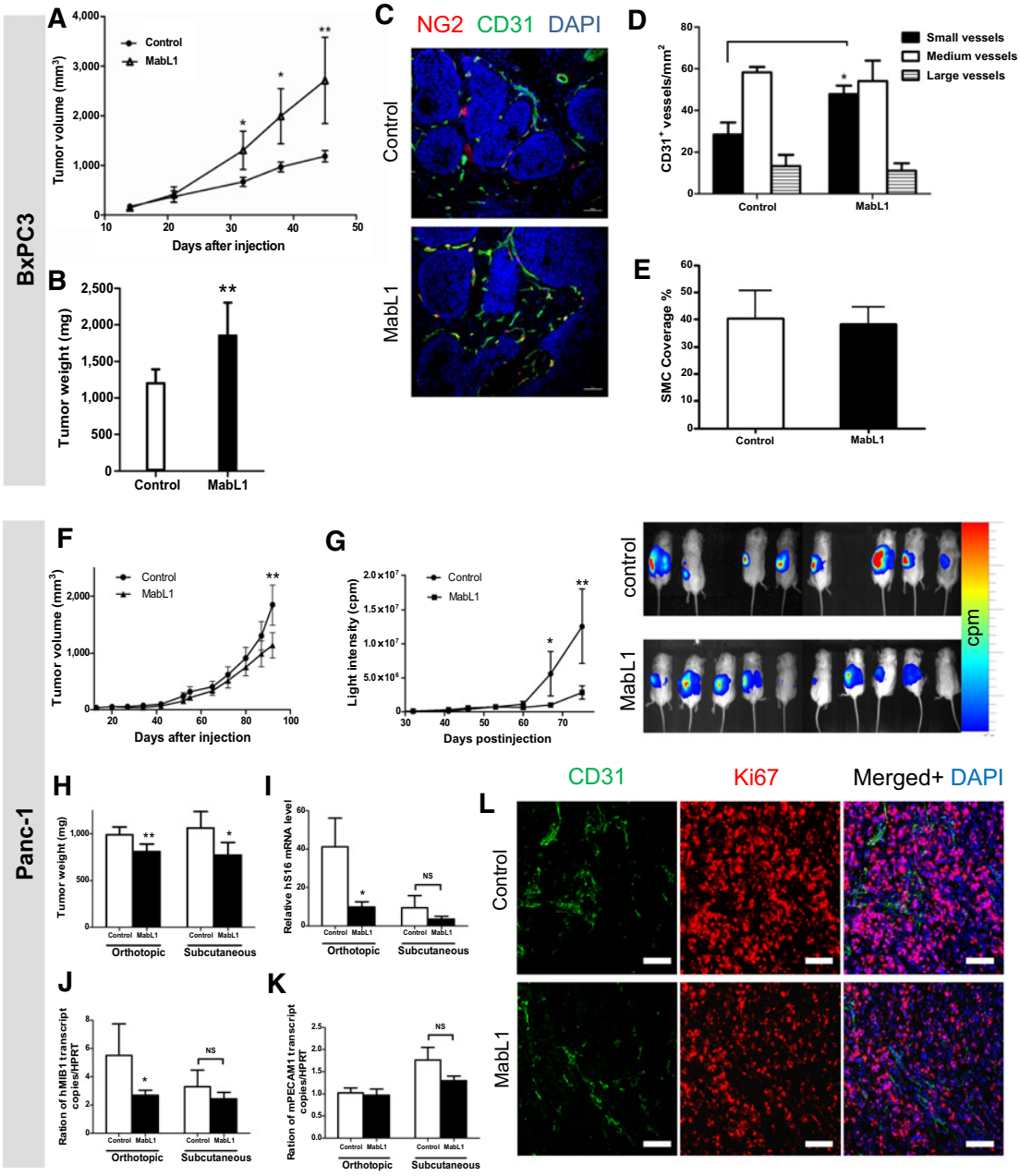

Figure 7.

Effect of CXCL4L1 blockade on *in vivo* pancreatic tumor development. **A,** tumor development in subcutaneously implanted BxPC3 cells ($n = 12$/group) and followed by caliper measurements in MabL1 or control antibody–treated animals. Treated tumors were significantly larger (**, $P < 0.01$). **B,** on the day of sacrifice, tumors were excised and weighted (**, $P < 0.01$). **C,** immunofluorescence staining for CD31 and NG2 on subcutaneous BxPC3 tumor section from control and MabL1-treated mice. **D,** quantification of vessel density grouped in small (<10 μm^2), medium (10–100 μm^2), or large $CD31^+$ vessels (>100 μm^2; $n = 5$ tumors/group, 10 pictures/tumor). MabL1-treated mice have significantly more small-diameter vessels in tumors compared with untreated controls (*, $P < 0.05$). **E,** quantification of SMC coverage. **F,** Panc-1 cells implanted subcutaneously or orthotopically by direct intrapancreatic injection in Rag2 γ/c mice and treated with MabL1 or with the control antibody. MabL1-treated mice with subcutaneously implanted cells had significantly smaller tumors (**, $P < 0,01$). **G,** bioluminescent imaging on orthotopic PANC-1-LucFirefly tumors using the Photon Imager (Biospace). Analysis by M3Vision software and represented as total flux measurements in count per minute. **H,** weights recorded from the excised tumors at sacrifice day 75 and 92 for orthotopic and subcutaneous tumors, respectively (**, $P < 0,01$; *, $P < 0.05$). **I,** quantification of lung metastasis in subcutaneously and orthotopically implanted mice by qRT-PCR for the human *S16* gene ($n = 10$ lungs/group; *, $P < 0.05$). m*HPRT1*, housekeeping gene. **J** and **K,** qRT-PCR analyses for human *MIB1* (**J**) and mouse *PECAM1* (**K**) in tumors (*, $P < 0.05$). **L,** immunofluorescence staining for mouse CD31 and human Ki67 on orthotopic tumor sections. Scale bar, 50 μm. Error bars, SEM.

It is to emphasize that CXCL4L1 or CXCL4 expression is not uniform for all pancreatic carcinoma cell lines tested. When CXCL4L1 or CXCL4 were analyzed in pancreatic carcinoma cells *in vitro* or after tumor implantation, two of the cell lines (BxPC3 and Panc-1) expressed increased levels of CXCL4L1 but not of CXCL4 *in vivo*. On the contrary, another cell line (Mia PaCa-2) overexpressed already *in vitro* CXCL4 but not CXCL4L1, and this was further increased in tumors generated after implantation in mice. Thus, CXCL4 may also have a role in PDAC physiopathology.

Expression of CXCL4L1 was also evidenced in other tumor types, such as colon tumors or esophageal cancer (31). Endometriosis-associated ovarian cancer seems to express decreased levels of CXCL4L1 (and CXCL4) in comparison with normal endometrium and endometriosis lesion, but only in tumor-associated macrophages (32).

Anti-CXCL4L1 antibodies were able to target metastatic lesions. This suggests that CXCL4L1 could be used for tumor targeting. However, mice do not express CXCL4L1, and in humans, targeting of CXCL4L1 may also affect normal cells, which would not be appropriate for tumor-targeting applications. CXCL4L1 diffuses much better than CXCL4 and, therefore, may not stay within the tumor tissue. Thus, further experiments are needed to validate CXCL4L1 for tumor-targeting approaches.

Functional data indicate that CXCL4L1 has no effect on proliferation, migration, or survival when tumor cells do not express CXCR3 protein, as is the case for BxPC3. Furthermore, significant effects on endothelial cell proliferation, migration, survival or tube formation, and cell signaling were observed after CXCL4L1 stimulation, which is in agreement with previous studies. Endothelial cell–expressed CXCR3 has been proposed to mediate the antiangiogenic effects of CXCL4 and CXCL4L1 (6, 33). Alternatively, CXCL4L1 may bind to an, as yet, unknown receptor.

We next investigated the role of endogenous CXCL4L1 in PDAC development. Transgenic mice models using conditional expression of mutant K-ras and p53 allele or TGFβ receptor seem to better recapitulate the multistage PDAC developmental process (34, 35) than implant models. However, CXCL4L1 is not present in mice, and thus, experiments aimed at blocking endogenous CXCL4L1 cannot be performed in these models.

In BxPC3 tumor xenografts, which do not express CXCR3 protein, blockade of endogenous CXCL4L1 resulted in an increase in tumor development. This is in agreement with an effect on the tumor stroma. In contrast, in Panc-1 tumor xenografts, which express high levels of CXCR3, the blockade of endogenous CXCL4L1 led to a decreased tumor development. Furthermore, we observed that CXCR3-A is mainly upregulated in Panc-1 cells *in vivo*. This is reinforced by functional studies that show that CXCR3 knockdown diminishes Panc-1 cell proliferation. The observation that tumors cells, which express CXCR3-A, exhibit an increase in tumor cell survival and proliferation is in line with our data (36). Furthermore, CXCR3 has intrinsically pro-metastatic activity.

All in all, our work establishes CXCL4L1 as a novel regulator of pancreatic tumor development that not only acts on the tumor microenvironment but also directly on tumor cells themselves. Expression of CXCL4L1 in tumor cells is controlled by stroma–tumor cell interactions and by epigenetic regulations. Further work is required to fully understand the specific microenvironmental and epigenetic mechanisms that regulate CXCL4L1 expression in tumor cells.

Disclosure of Potential Conflicts of Interest

No potential conflicts of interest were disclosed.

Disclaimer

The funders had no role in study design, data collection and analysis, decision to publish, or in the preparation of the manuscript.

Authors' Contributions

Conception and design: C. Quemener, A. Dubrac, F. Soulet, L. Dumartin, A. Lomri, A.-M. Khatib, M. Hagedorn, H. Prats, A. Bikfalvi

Development of methodology: K. Boyé, A. Dubrac, F. Soulet, L. Dumartin, T. Daubon, M. Hagedorn

Acquisition of data (provided animals, acquired and managed patients, provided facilities, etc.): C. Quemener, J. Baud, K. Boyé, A. Dubrac, F. Soulet, L. Dumartin, M. Sire, R. Grepin, F. Rayne, A. Couvelard, M. Hagedorn

Analysis and interpretation of data (e.g., statistical analysis, biostatistics, computational analysis): C. Quemener, J. Baud, K. Boyé, A. Dubrac, C. Billottet, F. Soulet, L. Dumartin, M. Sire, K. Clarke, A.-M. Khatib, M. Hagedorn, H. Prats, A. Bikfalvi

Writing, review, and/or revision of the manuscript: J. Baud, K. Boyé, A. Dubrac, C. Billottet, V. Castronovo, A.-M. Khatib, M. Hagedorn, A. Bikfalvi

Administrative, technical, or material support (i.e., reporting or organizing data, constructing databases): C. Billottet, F. Darlot, M. Sire, H. Wodrich, R. Pineau, M. Schilling, V. Castronovo, S.-C. Sue

Study supervision: A. Bikfalvi

Grant Support

This work was supported by grants from Agence Nationale de la Recherche, the Association de la Recherche sur le Cancer, the Ligue Nationale contre Cancer (A. Bikfalvi), Institut National du Cancer (INCA; to A. Bikfalvi and H. Prats), and ANR (M. Hagedorn). This work was also supported by a PhD fellowship from INCA (A. Dubrac) and the Ministère de la Recherche and Fondation pour la Recherche Médicale (K. Boye and L. Dumartin).

The costs of publication of this article were defrayed in part by the payment of page charges. This article must therefore be hereby marked *advertisement* in accordance with 18 U.S.C. Section 1734 solely to indicate this fact.

Received October 15, 2015; revised July 9, 2016; accepted August 12, 2016; published OnlineFirst September 9, 2016.

References

1. Struyf S, Burdick MD, Peeters E, Van den Broeck K, Dillen C, Proost P, et al. Platelet factor-4 variant chemokine CXCL4L1 inhibits melanoma and lung carcinoma growth and metastasis by preventing angiogenesis. Cancer Res 2007;67:5940–8.
2. Struyf S, Burdick MD, Proost P, Van Damme J, Strieter RM. Platelets release CXCL4L1, a nonallelic variant of the chemokine platelet factor-4/CXCL4 and potent inhibitor of angiogenesis. Circ Res 2004; 95:855–7.
3. Dubrac A, Quemener C, Lacazette E, Lopez F, Zanibellato C, Wu WG, et al. Functional divergence between 2 chemokines is conferred by single amino acid change. Blood 2010;116:4703–11.
4. Lasagni L, Grepin R, Mazzinghi B, Lazzeri E, Meini C, Sagrinati C, et al. PF-4/CXCL4 and CXCL4L1 exhibit distinct subcellular localization and a differentially regulated mechanism of secretion. Blood 2007;109:4127–34.
5. Kuo JH, Chen YP, Liu JS, Dubrac A, Quemener C, Prats H, et al. Alternative C-terminal helix orientation alters chemokine function:

structure of the anti-angiogenic chemokine, CXCL4L1. J Biol Chem 2013;288:13522–33.
6. Struyf S, Salogni L, Burdick MD, Vandercappellen J, Gouwy M, Noppen S, et al. Angiostatic and chemotactic activities of the CXC chemokine CXCL4L1 (platelet factor-4 variant) are mediated by CXCR3. Blood 2011;117:480–8.
7. Billottet C, Quemener C, Bikfalvi A. CXCR3, a double-edged sword in tumor progression and angiogenesis. Biochim Biophys Acta 2013;1836: 287–95.
8. Van Raemdonck K, Van den Steen PE, Liekens S, Van Damme J, Struyf S. CXCR3 ligands in disease and therapy. Cytokine Growth Factor Rev 2015;26:311–27.
9. Karin N, Wildbaum G, Thelen M. Biased signaling pathways via CXCR3 control the development and function of CD4+ T cell subsets. J Leukoc Biol 2016;99:857–62.
10. Vandercappellen J, Noppen S, Verbeke H, Put W, Conings R, Gouwy M, et al. Stimulation of angiostatic platelet factor-4 variant (CXCL4L1/PF-4var) versus inhibition of angiogenic granulocyte chemotactic protein-2 (CXCL6/GCP-2) in normal and tumoral mesenchymal cells. J Leukoc Biol 2007;82:1519–30.
11. Vandercappellen J, Liekens S, Bronckaers A, Noppen S, Ronsse I, Dillen C, et al. The COOH-terminal peptide of platelet factor-4 variant (CXCL4L1/PF-4var47-70) strongly inhibits angiogenesis and suppresses B16 melanoma growth in vivo. Mol Cancer Res 2010;8:322–34.
12. Van Raemdonck K, Berghmans N, Vanheule V, Bugatti A, Proost P, Opdenakker G, et al. Angiostatic, tumor inflammatory and anti-tumor effects of CXCL4(47-70) and CXCL4L1(47-70) in an EGF-dependent breast cancer model. Oncotarget 2014;5:10916–33.
13. Hagedorn M, Javerzat S, Gilges D, Meyre A, de Lafarge B, Eichmann A, et al. Accessing key steps of human tumor progression in vivo by using an avian embryo model. Proc Natl Acad Sci U S A 2005;102:1643–8.
14. Dumartin L, Quemener C, Laklai H, Herbert J, Bicknell R, Bousquet C, et al. Netrin-1 mediates early events in pancreatic adenocarcinoma progression, acting on tumor and endothelial cells. Gastroenterology 2010;138:1595–606.
15. Hedrich H, Bullock G, Petrusz P, eds. The Laboratory Mouse. 2nd ed. London: Academic Press, 2012.
16. Platonova N, Miquel G, Regenfuss B, Taouji S, Cursiefen C, Chevet E, et al. Evidence for the interaction of fibroblast growth factor-2 with the lymphatic endothelial cell marker LYVE-1. Blood 2013;121:1229–37.
17. Liu ZQ, Mahmood T, Yang PC. Western blot: technique, theory and trouble shooting. N Am J Med Sci 2014;6:160.
18. Clarke K, Daubon T, Turan N, Soulet F, Mohd Zahari M, Ryan KR, et al. Inference of low and high-grade glioma gene regulatory networks delineates the role of Rnd3 in establishing multiple hallmarks of cancer. PLoS Genet 2015;11:e1005325.
19. Segara D, Biankin AV, Kench JG, Langusch CC, Dawson AC, Skalicky DA, et al. Expression of HOXB2, a retinoic acid signaling target in pancreatic cancer and pancreatic intraepithelial neoplasia. Clin Cancer Res 2005;11: 3587–96.
20. Ishikawa M, Yoshida K, Yamashita Y, Ota J, Takada S, Kisanuki H, et al. Experimental trial for diagnosis of pancreatic ductal carcinoma based on gene expression profiles of pancreatic ductal cells. Cancer Sci 2005; 96:387–93.
21. Hashimoto K, Oreffo RO, Gibson MB, Goldring MB, Roach HI. DNA demethylation at specific CpG sites in the IL1B promoter in response to inflammatory cytokines in human articular chondrocytes. Arthritis Rheum 2009;60:3303–13.
22. Ramaswamy S, Tamayo P, Rifkin R, Mukherjee S, Yeang CH, Angelo M, et al. Multiclass cancer diagnosis using tumor gene expression signatures. Proc Natl Acad Sci U S A 2001;98:15149–54.
23. Buchholz M, Braun M, Heidenblut A, Kestler HA, Kloppel G, Schmiegel W, et al. Transcriptome analysis of microdissected pancreatic intraepithelial neoplastic lesions. Oncogene 2005;24:6626–36.
24. Beltran AS, Sun X, Lizardi PM, Blancafort P. Reprogramming epigenetic silencing: artificial transcription factors synergize with chromatin remodeling drugs to reactivate the tumor suppressor mammary serine protease inhibitor. Mol Cancer Ther 2008;7:1080–90.
25. Hellebrekers DM, Castermans K, Vire E, Dings RP, Hoebers NT, Mayo KH, et al. Epigenetic regulation of tumor endothelial cell anergy: silencing of intercellular adhesion molecule-1 by histone modifications. Cancer Res 2006;66:10770–7.
26. Seo J, Kim YO, Jo I. Differential expression of stromal cell-derived factor 1 in human brain microvascular endothelial cells and pericytes involves histone modifications. Biochem Biophys Res Commun 2009;382:519–24.
27. Sowinska A, Jagodzinski PP. RNA interference-mediated knockdown of DNMT1 and DNMT3B induces CXCL12 expression in MCF-7 breast cancer and AsPC1 pancreatic carcinoma cell lines. Cancer Lett 2007;255: 153–9.
28. Pakneshan P, Szyf M, Rabbani SA. Methylation and inhibition of expression of uPA by the RAS oncogene: divergence of growth control and invasion in breast cancer cells. Carcinogenesis 2005;26:557–64.
29. Sato N, Fukushima N, Matsubayashi H, Goggins M. Identification of maspin and S100P as novel hypomethylation targets in pancreatic cancer using global gene expression profiling. Oncogene 2004;23:1531–8.
30. Sato N, Maehara N, Su GH, Goggins M. Effects of 5-aza-2′-deoxycytidine on matrix metalloproteinase expression and pancreatic cancer cell invasiveness. J Natl Cancer Inst 2003;95:327–30.
31. Verbeke H, De Hertogh G, Li S, Vandercappellen J, Noppen S, Schutyser E, et al. Expression of angiostatic platelet factor-4var/CXCL4L1 counterbalances angiogenic impulses of vascular endothelial growth factor, interleukin-8/CXCL8, and stromal cell-derived factor 1/CXCL12 in esophageal and colorectal cancer. Hum Pathol 2010;41:990–1001.
32. Furuya M, Tanaka R, Miyagi E, Kami D, Nagahama K, Miyagi Y, et al. Impaired CXCL4 expression in tumor-associated macrophages (TAMs) of ovarian cancers arising in endometriosis. Cancer Biol Ther 2012;13: 671–80.
33. Lasagni L, Francalanci M, Annunziato F, Lazzeri E, Giannini S, Cosmi L, et al. An alternatively spliced variant of CXCR3 mediates the inhibition of endothelial cell growth induced by IP-10, Mig, and I-TAC, and acts as functional receptor for platelet factor 4. J Exp Med 2003;197:1537–49.
34. Guerra C, Schuhmacher AJ, Canamero M, Grippo PJ, Verdaguer L, Perez-Gallego L, et al. Chronic pancreatitis is essential for induction of pancreatic ductal adenocarcinoma by K-Ras oncogenes in adult mice. Cancer Cell 2007;11:291–302.
35. Cook N, Olive KP, Frese K, Tuveson DA. K-Ras-driven pancreatic cancer mouse model for anticancer inhibitor analyses. Methods Enzymol 2008; 439:73–85.
36. Giuliani N, Bonomini S, Romagnani P, Lazzaretti M, Morandi F, Colla S, et al. CXCR3 and its binding chemokines in myeloma cells: expression of isoforms and potential relationships with myeloma cell proliferation and survival. Haematologica 2006;91:1489–97.